Electronic Supplementary Information for

Topology Design of Digital Metamaterials for Ultra-Compact Integrated Photonic Devices Based on Mode Manipulation

Han Ye[1,*], Yanrong Wang[1], Shuhe Zhang[1], Danshi Wang[1], Yumin Liu[1], Mingchao Wang[2,*], Qiming Zhang[3,*]

[1] State Key Laboratory of Information Photonics and Optical Communications, Beijing University of Posts and Telecommunications, Beijing 100876, China

[2] Centre for Theoretical and Computational Molecular Science, Australian Institute for Bioengineering and Nanotechnology, The University of Queensland, St Lucia, QLD 4072, Australia

[3] Centre for Artificial-Intelligence Nanophotonics, School of Optical-Electrical and Computer Engineering, University of Shanghai for Science and Technology, Shanghai 200093, China.

* Corresponding author: Han_ye@bupt.edu.cn (H. Ye);

mingchao.wang@uq.edu.eu (M. Wang);

qimingzhang@usst.edu.cn (Q. Zhang).

Table S1. Air and silicon pixel amount in the designed digital metamaterials.

	Air	Silicon		Air	Silicon
2D designs					
TE0-to-TE1	556	2027	TE0-to-TE2	613	1970
TE0-to-TE3	554	2029	TE1-to-TE2	628	1955
TE1-to-TE3	341	2242	TE2-to-TE3	374	2209
Diode	760	1823	Demultiplexer	1046	2923
Quasi-3D designs					
TE0-to-TE1	803	1780			
Diode	983	1600	Demultiplexer	834	3135

Table S2. Comparison between Ref. 1 and this work. Footprint and transmission efficiencies at center wavelength obtained from 2D simulations are listed for six mode conversions. It is noted that the distribution of refractive index (RI) in Ref. 1 had continuous regions, while in our design only air and silicon can be found.

	Footprint	TE0-to-TE1	TE0-to-TE2	TE0-to-TE3	TE1-to-TE2	TE1-to-TE3	TE2-to-TE3
Ref. 1	$1.55\lambda^2$ Continuous RI	99.3%	98.3%	90.6%	96.8%	86.3%	80.1%
This work	$0.645\lambda^2$ Binary RI	98.4%	96.7%	88.2%	95.3%	88.7%	85.3%

Table S3. Comparison between reported TE0-to-TE1 mode converter and this work. Transmission efficiencies at center wavelength obtained from 3D simulations are listed.

	Scheme	Footprint	TE0-to-TE1 (3D)
Ref. 2	Photonic crystal	~6.3μm×3.2μm	3D Opt: ~80% Quasi-3D Opt: ~60%
Ref. 3	Taper waveguide	~18.6μm×2.8μm	98.6%
Ref. 4	Ge/Si pattern	1.0μm×1.55μm	~91%
Ref. 5	Digital metamaterial	1.1μm×2.3μm 1.0μm×3.1μm	57% 37%
This work	Digital metamaterial	1.0μm×1.55μm	52.7%

Table S4. Comparison between reported reciprocal optical diodes and this work. Footprint, transmission efficiencies at center wavelength and contrast ratio (T_{forw}/T_{back}) obtained from 3D simulations are listed.

	Scheme	Footprint	Forward (3D)	Backward (3D)	Contrast ratio
Ref. 6	Ag splitter	4.0μm×0.65μm	62%	0.3%	206
Ref. 7	Partially etching	7.0μm×1.0μm	62%	0.53%	117
Ref. 8	Digital metamaterial	3.0μm×3.0μm	TE: 71.1% TM: 91.1%	1.8% 3.2%	40 28.5
Ref. 5	Digital metamaterial	1.1μm×2.3μm 1.0μm×3.1μm	57% 37%	1.8% 0.9%	32 41
This work	Digital metamaterial	1.0μm×1.55μm	43.1%	0.47%	91.7

Table S5. Comparison between inversely designed mode-order demultiplexers and this work. Channel number, footprint, insertion loss at center wavelength and contrast ratio obtained from 3D simulations are listed.

	Channel number	Footprint	Insertion loss (3D)	Contrast ratio
Ref. 9	2 3	4.22μm×2.6μm 6.08μm×4.93μm	-0.25dB	~17dB
Ref. 10	4	5.4μm×6.0μm	< -1.5dB	18 dB
Ref. 11	3	3.6μm *4.8μm	< -1.5dB	22dB
This work	2	1.55μm×1.55μm	-2.2dB	14.7dB

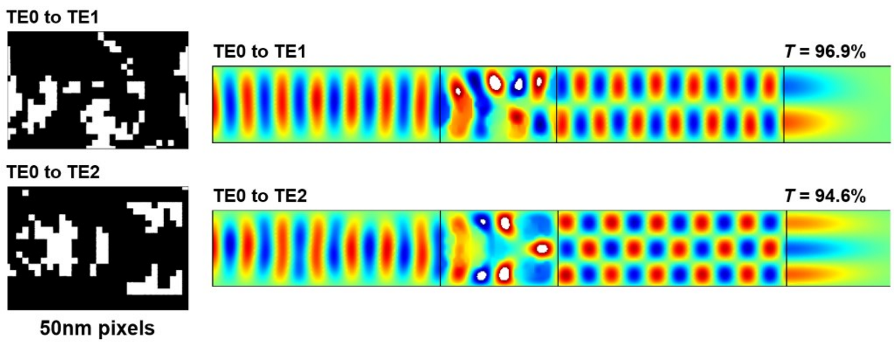

Figure S1. Designs for mode converters (TE0-to-TE1 and TE0-to-TE2) with 50nm pixels and corresponding magnetic fields simulated at center wavelength.

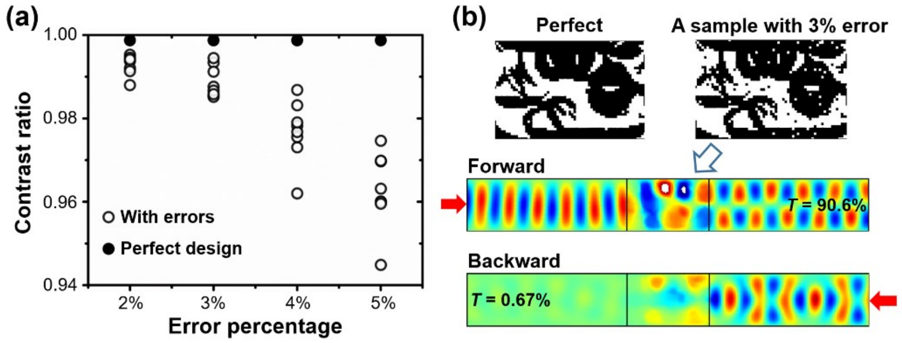

Figure S2. Contrast ratio of reciprocal optical diode with random errors. (b) Structure and magnetic field of a diode sample with 3% error. This sample is the one with the lowest contrast ratio among 8 samples with 3% error percentage.

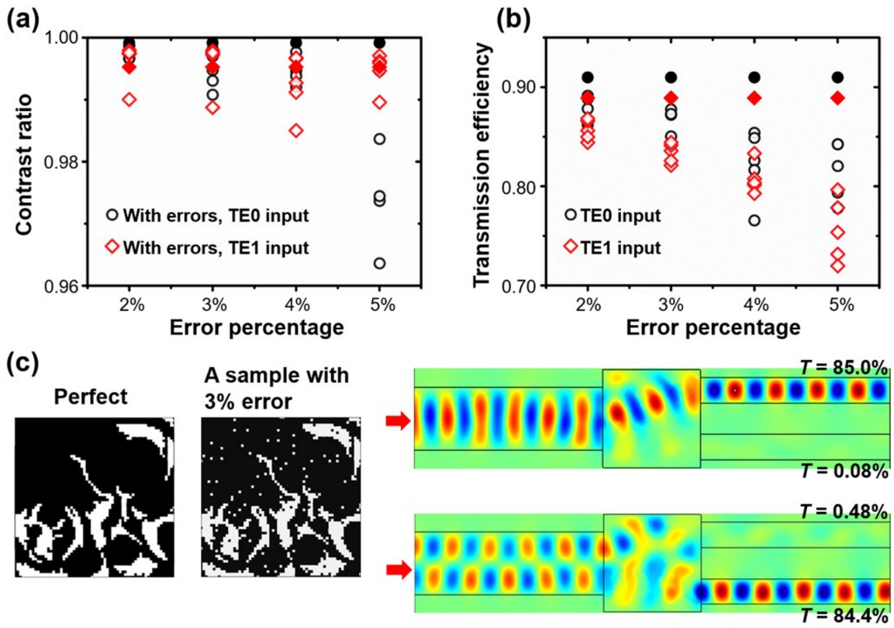

Figure S3. Contrast ratio and transmission efficiencies of demultiplexer with random errors. (b) Structure and magnetic field of a diode sample with 3% error. This sample is the one with the lowest contrast ratio among 5 samples with 3% error percentage.

References

1. J. Lu, J. Vuckovic, Objective-first design of high-efficiency, small-footprint couplers between arbitrary nanophotonic waveguide modes, Opt. Express 20 (2012) 7221.
2. L.H. Frandsen, Y. Elesin, L.F. Frellsen, M. Mitrovic, Y. Ding, O. Sigmund, K. Yvind, Topology optimized mode conversion in a photonic crystal waveguide fabricated in silicon-on insulator material, Opt. Express 22 (2014) 8525.
3. D. Chen, X. Xiao, L. Wang, Y. Yu, W. Liu, Q. Yang, Low-loss and fabrication tolerant silicon mode order converters based on novel compact tapers, Opt. Express 23 (2015) 11152.
4. H. Ye, F. Yu, Y. Liu, Z. Yu, J. Li, D.F. Zhu, B.D. Su, W.B. Xu, Ultra-Compact Waveguide-Integrated TE-Mode Converters With High Mode Purity by Designing Ge/Si Patterns, IEEE Photon. J. 11 (2019) 6602208
5. F. Callewaert, S. Butun, Z. Li, K. Aydin, Inverse design of an ultra-compact broadband optical diode based on asymmetric spatial mode conversion, Sci. Rep. 6 (2016) 32577.
6. J. Li, H. Ye, Z. Yu, Y. Liu, Design of a broadband reciprocal optical diode in a silicon waveguide assisted by silver surface plasmonic splitter, Opt. Express 25 (2017) 19129.
7. D. Zhu, J. Zhang, H. Ye, Z. Yu, Y. Liu, Design of a broadband reciprocal optical diode in multimode silicon waveguide by partial depth etching, Opt. Commun. 418 (2018) 88.
8. B. Shen, R. Polson, R. Menon, Integrated digital metamaterials enables ultra-compact optical diodes, Opt. Express 23 (2015) 10847.
9. L.F. Frellsen, Y. Ding, O. Sigmund, L.H. Frandsen, Topology optimized mode multiplexing in silicon-on-insulator photonic wire waveguides, Opt. Express 24 (2016) 16866.
10. H. Xie, Y. Liu, S. Wang, Y. Wang, Y. Yao , Q. Song, J. Du , Z. He, K. Xu, Highly Compact and Efficient Four-Mode Multiplexer Based on Pixelated Waveguides, IEEE Photon. Technol. Lett. 32 (2020) 166.
11. W. Chang, L. Lu, X. Ren, L. Lu, M. Cheng, D. Liu, .M.M. Zhang, An Ultracompact Multimode Waveguide Crossing Based on Subwavelength Asymmetric Y-Junction, IEEE Photon. J. 10 (2018) 4501008.